Microchannels and Minichannels - 2004
June 17-19, 2004, Rochester, New York, USA

ICMM2004 – 2368

MODELING AND DESIGN OF MICRO GROOVE FALLING FILM EVAPORATORS

Shohei Hasebe[1], Naoki Shikazono[2] and Nobuhide Kasagi[3]

[1] The University of Tokyo, 7-3-1 Hongo, Bunkyo-ku, Tokyo, Japan; E-mail: hasebe@thtlab.t.u-tokyo.ac.jp
[2] The University of Tokyo, 7-3-1 Hongo, Bunkyo-ku, Tokyo, Japan; E-mail: shika@thtlab.t.u-tokyo.ac.jp
[3] The University of Tokyo, 7-3-1 Hongo, Bunkyo-ku, Tokyo, Japan; E-mail: kasagi@thtlab.t.u-tokyo.ac.jp

ABSTRACT

In the present study, heat transfer in a falling film micro groove evaporator has been simulated by an analytical model. The flow and thermal fields were divided in two regions, i.e. macroscopic flow inside the groove and the microscopic flow where intensive evaporation takes place at the thin film interline region. For the micro region model, pressure in the liquid film was expressed as a sum of surface tension and disjoining pressure effects. The film thickness profile was obtained by solving the 4th order differential equation by Runge-Kutta method. Then, this micro region model was combined with the macro region model. Macro region model solves one dimensional bulk flow inside the groove with gravitational effect taken into account. Constant curvature of the liquid vapor surface was assumed for the macro flow. It is shown that the gravitational force is essential for providing the liquid to wide range of heat transfer area. Thus, diverging branch evaporator is investigated. It is demonstrated that this concept has large potentiality for improving the performance of the micro groove falling film evaporator.

INTRODUCTION

Since thin liquid films can promote very rapid and intensive heat and mass transfer, falling film systems have been attracting large attention in the area of extraction, absorption, phase change and exothermic processes. With a micro-grooved surface, falling film systems can generate thin liquid films with thickness less than 100 μm on a solid wall. Thus, falling film system is expected to be one of the key technologies for developing micro or mini heat exchangers and reactors. Figure 1 shows the schematic view of the falling film evaporator with triangular grooves. In case of micro groove evaporator, it is known that intensive evaporation can be achieved at the interline region where very thin liquid film is formed adjacent to the adsorbed film (see Wayner, 1997, 1999). However, this strong evaporation occurs at a very limited area. For example, the length scale of this strong evaporation region is in a submicron range. Therefore, the main challenge in

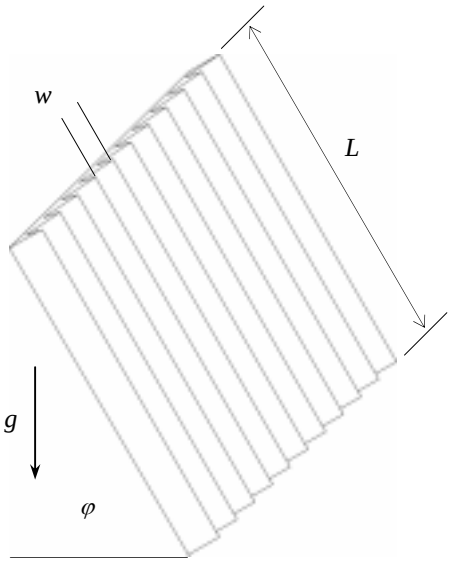

Fig. 1 Schematic view of the falling film evaporator

developing a compact micro groove evaporator is to spotlight and emerge such microscopic strong evaporation in a macroscopic heat transfer surface. It is expected that this can be achieved by optimizing the width, length, path patterns and directions of the micro grooves on the surface.

In the present study, evaporation in a grooved surface is simulated analytically extending the method proposed by previous researchers, e.g. Wayner, et al. (1976, 1982), Kamotani (1978) and Stephan and Busse (1992) etc. In the following sections, the model equations for the micro and macro regions are presented. Finally, the model is applied to micro groove falling film evaporators. A concept that can improve the performance of the falling film evaporator, i.e. diverging branch evaporator, is investigated.

MODELING OF FALLING FILM EVAPORATOR

Micro Region Model

In the present study, the analytical model described by Stephan and Busse (1992) is adopted for the micro region. Since Reynolds number is very small and the surface tension becomes dominant in this scale, gravity is ignored in the micro model. Figure 2 shows the meniscus of the liquid captured in a triangular groove, and Fig. 3 shows the enlarged view of the micro region. In this study, right triangular shape is adopted for the cross section of the groove because of the simplicity of analytical treatment. Intensive evaporation takes place at the so-called interline region where liquid film gets very thin. The heat flux $\dot{q}$ in the liquid film is assumed to be one dimensional in the wall normal direction and can be written as

$$\dot{q} = (T_W - T_{iv}) \Bigg/ \left(\frac{\delta}{\lambda_l} + \frac{T_{sat}\sqrt{(2\pi R_g T_{sat})}}{h_{fg}^2 \rho_v} \frac{(2-f)}{2f} \right) \tag{1}$$

where the second term in the denominator corresponds to the interfacial heat resistance. The evaporation coefficient f was set as $f = 1$. Constant wall temperature T_w is assumed in this study. The temperature at the vapor side of the interface T_{iv} is related to the saturation temperature T_{sat} by the following relation;

$$T_{iv} = T_{sat}\left(1 + \frac{p_c}{h_{fg}\rho_l}\right) \tag{2}$$

where p_c is the pressure difference between vapor and liquid phases;

$$p_c = p_v - p_l = K\sigma + \frac{A}{\delta^3}. \tag{3}$$

The first term describes the surface tension effect and the second term corresponds to the disjoining pressure effect. The curvature K can be expressed using film thickness δ as

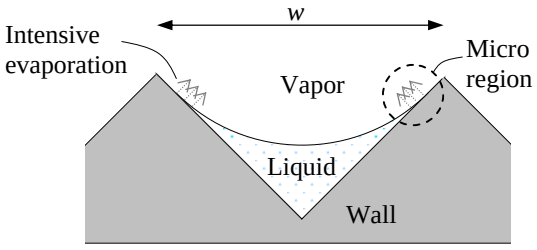

Fig. 2 Meniscus of liquid in a right triangular groove

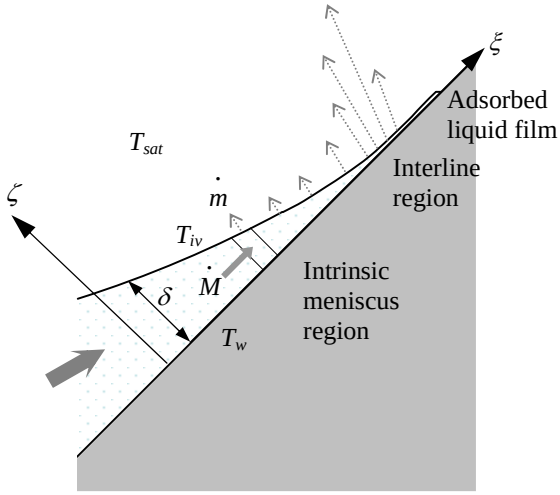

Fig. 3 Enlarged view of the micro region

$$K = \frac{\dfrac{d^2\delta}{d\xi^2}}{\left\{1 + \left(\dfrac{d\delta}{d\xi}\right)^2\right\}^{3/2}}. \tag{4}$$

This pressure distribution due to the film thickness profile pulls the liquid to the strong evaporating interline region until it balances with the viscous drag of the flow.

The local and mean velocity profiles u and $\bar{u}$ in a laminar boundary layer are given as

$$u = \frac{1}{\mu}\frac{dp_l}{d\xi}\left(\frac{\zeta^2}{2} - \delta\zeta\right), \tag{5}$$

$$\bar{u} = \frac{1}{\delta}\int_0^\delta u d\zeta - \frac{\delta^2}{3\nu_l\rho_l}\frac{dp_l}{d\xi}. \tag{6}$$

Then the mass flow rate $\dot{M}$ $(= \bar{u}\delta\rho_l)$ can be obtained using Eq. (6);

$$\dot{M} = -\frac{\delta^3}{3\nu_l}\frac{dp_l}{d\xi}. \tag{7}$$

Thus, evaporation rate $\dot{m}$ is obtained as follows:

$$\dot{m}'' = -\frac{dM''}{d\xi} = \frac{1}{3\nu_l}\frac{d}{d\xi}\left(\delta^3 \frac{dp_l}{d\xi}\right). \tag{8}$$

Assuming that vapor pressure p_v is constant, the liquid phase pressure gradient is related to the capillary pressure gradient as

$$\frac{dp_l}{d\xi} = -\frac{dp_c}{d\xi}. \tag{9}$$

Thus, one obtains the expression for the heat flux as

$$q'' = -\frac{h_{fg}}{3\nu_l}\frac{d}{d\xi}\left(\delta^3 \frac{dp_c}{d\xi}\right). \tag{10}$$

Combining Eqs. (1), (2), (3), (4) and (10), the fourth order differential equation for the liquid thickness δ is obtained;

$$\frac{\sigma}{3\mu_l}\frac{d}{d\xi}\left\{\delta^3 \frac{d}{d\xi}\left(\frac{\dfrac{d^2\delta}{d\xi^2}}{\left\{1+\left(\dfrac{d\delta}{d\xi}\right)^2\right\}^{3/2}} + \frac{A}{\sigma\delta^3}\right)\right\} = \frac{T_{sat}-T_w + \dfrac{T_{sat}\sigma}{h_{fg}\rho_l}\left[\dfrac{\dfrac{d^2\delta}{d\xi^2}}{\left\{1+\left(\dfrac{d\delta}{d\xi}\right)^2\right\}^{3/2}} + \dfrac{A}{\sigma\delta^3}\right]}{\rho_l h_{fg}\left(\dfrac{\delta}{\lambda_l} + \dfrac{T_{sat}\sqrt{2\pi R_g T_{sat}}}{h_{fg}^2\rho_v}\dfrac{2-f}{2f}\right)}. \tag{11}$$

In order to solve Eq. (11), following four variables are introduced:

$$z_1 = \delta, \tag{12}$$

$$z_2 = \frac{d\delta}{d\xi}, \tag{13}$$

$$z_3 = \frac{\dfrac{d^2\delta}{d\xi^2}}{\left\{1+\left(\dfrac{d\delta}{d\xi}\right)^2\right\}^{3/2}} + \frac{A}{\sigma\delta^3}, \tag{14}$$

$$z_4 = \frac{\sigma}{3\mu_l}\delta^3\frac{d}{d\xi}\left(\frac{\dfrac{d^2\delta}{d\xi^2}}{\left\{1+\left(\dfrac{d\delta}{d\xi}\right)^2\right\}^{3/2}} + \frac{A}{\sigma\delta^3}\right), \tag{15}$$

where variables z_1, z_2, z_3 and z_4 correspond to film thickness, film slope, capillary pressure and flow rate, respectively. Then Eq. (11) can be rewritten as a system of four first order differential equations as follows:

$$\frac{dz_1}{d\xi} = z_2, \tag{16}$$

$$\frac{dz_2}{d\xi} = \left(z_3 - \frac{A}{\sigma z_1^3}\right)\left(1+z_2^2\right)^{3/2}, \tag{17}$$

$$\frac{dz_3}{d\xi} = \frac{3\mu_l}{\sigma}\frac{z_4}{z_1^3}, \tag{18}$$

$$\frac{dz_4}{d\xi} = \frac{T_{sat}-T_w + \dfrac{T_{sat}\sigma}{h_{fg}\rho_l}z_3}{\rho_l h_{fg}\left(\dfrac{\delta}{\lambda_l} + \dfrac{T_{sat}\sqrt{2\pi R_g T_{sat}}}{h_{fg}^2\rho_v}\dfrac{2-f}{2f}\right)}. \tag{19}$$

This set of equations is integrated by fourth order Runge-Kutta method. The boundary conditions are shown in Fig. 4. At the macro and micro boundary, the film thickness gradient z_{2in} , and z_{3in} ($=p_c/\sigma$) are set as

$$z_{2in} = \tan\theta, \tag{20}$$

$$z_{3in} \approx K = 1/R_{in}. \tag{21}$$

In the present study, the slope of the vapor liquid interface at the macro-micro boundary is chosen as θ=30 degrees. It is confirmed from the preliminary calculations for θ=25~45 degrees that this condition doesn't affect the film thickness and the heat flux prediction at the interline region near the adsorbed thin film boundary. The film thickness z_{1in} and flow rate z_{4in} at the macro-micro boundary are chosen by iteration so that both film slope z_{2end} and flow rate z_{4end} become zero at the micro and adsorbed film boundary, i.e.

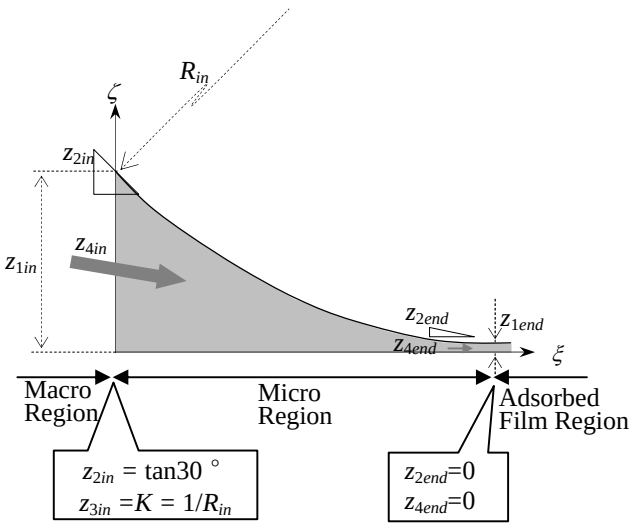

Fig. 4 Boundary conditions

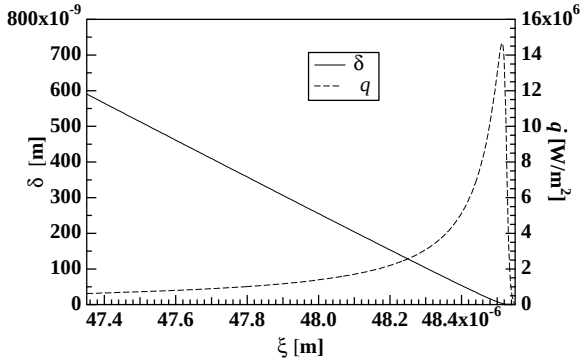

Fig. 5 Predicted film thickness and heat flux by the micro region model

$$z_{2end} = 0, \tag{22}$$

$$z_{4end} = 0. \tag{23}$$

Figure 5 shows the predicted film thickness and heat flux profile for R123 with T_w=303.15K and T_{sat}=298.15K. The dispersion constant was set as $A = 2.0\times10^{-21}$ J. As film thickness δ decreases, thermal resistance of liquid film is reduced and thus heat flux increases. However, as film thickness becomes much thinner, capillary pressure p_c increases dramatically due to the disjoining pressure effect. As seen from Eq. (2), temperature at the liquid-vapor interface T_{iv} increases for large p_c, and this suppresses evaporation at the absorbed film region. Extremely high heat flux ($\dot{q} > 1400$ W/cm^2) is observed at a very narrow area of the interline region, even for R123 which has relatively low thermal conductivity compared to water or ammonia. The film thickness is less than 100nm at the interline region.

Macro Region Model

Then, the micro region model is combined with the macro region model. Macro region model solves one dimensional bulk flow inside the groove, considering the effects of gravity, viscosity and surface tension forces. Heat transfer from the macro region is ignored in this study as a first order approximation. The schematic view of the flow along the groove is shown in Fig. 6. The shape of liquid-vapor interface is assumed to be circular arc. This curvature radius R is used as the boundary condition for the micro region model at each cross section of the groove.

Figure 7 shows the control volume for the macro region. Momentum balance of the flow inside the groove in the x direction can be expressed as

$$\Delta p_{surface\_tension} = \Delta p_{viscous} + \Delta p_{gravity}, \tag{24}$$

where viscous drag $\Delta p_{viscous}$ is given by the predictive method for stratified two phase pipe flows described by Taitel and Duckler (1976);

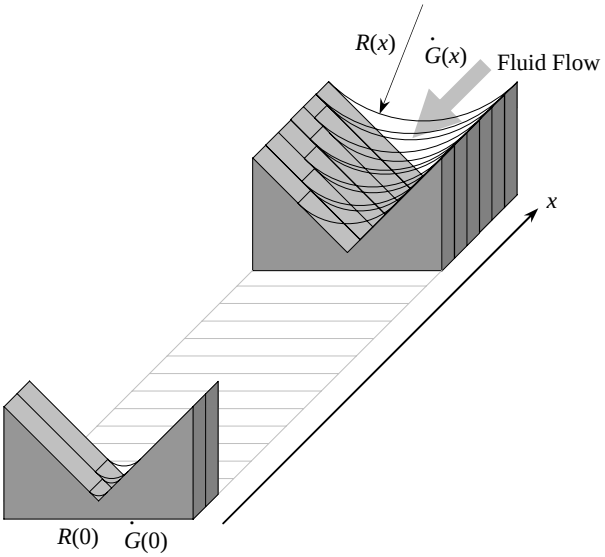

Fig. 6 Schematic view of the flow inside the groove

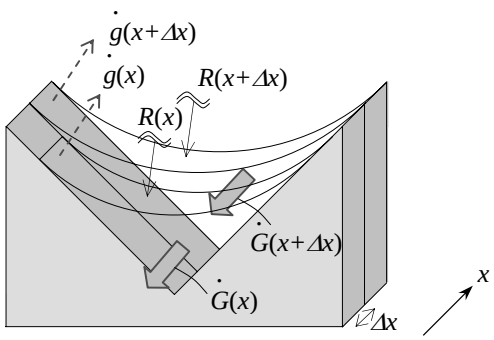

Fig. 7 Control volume for the macro region

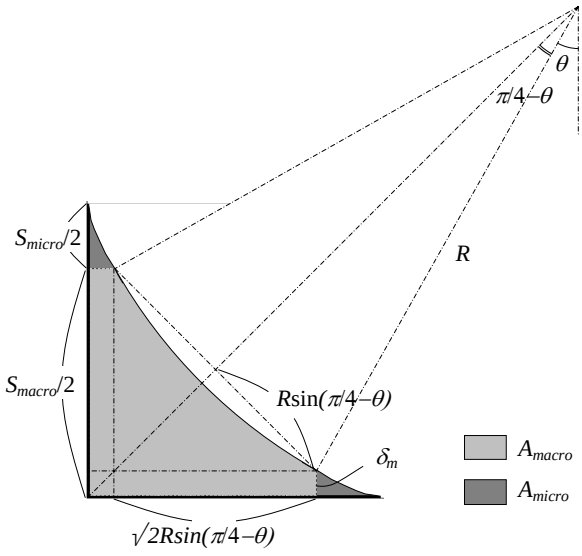

Fig. 8 Cross section of the groove

$$\Delta p_{viscous} = 4 f \frac{\Delta x}{D} \frac{\rho_l}{2} u_m^2, \tag{25}$$

where u_m is the mean liquid velocity inside the groove. For the friction factor,

$$f = \frac{24}{\mathrm{Re}_D} \tag{26}$$

is recommended for low Reynolds number laminar flows by Spedding and Hand (1997). The hydraulic diameter D is defined as

$$D = \frac{4\left(A_{macro} + A_{micro}\right)}{S_{macro} + S_{micro}}, \tag{27}$$

where S is the perimeter of the wet wall and A is the cross section of the liquid flow, as shown in Fig. 8.

Thus, pressure difference due to the surface tension force can be written as

$$\Delta p_{surface\_tension} = \frac{96}{\mathrm{Re}_D} \frac{\Delta x}{D} \frac{\rho}{2} u^2 - \rho g \Delta x \sin\varphi, \tag{28}$$

where φ is the angle of inclination of the surface respect to the horizontal plane (see Fig. 1).

Surface tension pressure difference $\Delta p_{surface\_tension}$ can be also expressed by the curvature radius R as

$$\Delta p_{surface\_tension} = \frac{\sigma}{R(x)} - \frac{\sigma}{R(x+\Delta x)}. \tag{29}$$

Thus, the curvature radius at the neighboring cross section $R(x+\Delta x)$ can be obtained from Eqs. (27) and (28) as

$$R(x+\Delta x) = \left(\frac{1}{R(x)} - \frac{\frac{96}{\mathrm{Re}_D} \frac{\Delta x}{D} \frac{\rho_l}{2} u_m^2 - \rho_l g \Delta x \sin\varphi}{\sigma} \right)^{-1}. \tag{30}$$

If the initial value of meniscus radius $R(0)$ is given at x=0, evaporation rate $\dot{g}(0)$, film thickness $\delta_m(0)$ at the macro-micro boundary, cross sectional area and perimeter length of the micro region, A_{micro} and $S_{micr,o}$ can be obtained from the micro region calculation. Then, one obtains the curvature radius and the flow rate at the next control volume. This procedure is continued in sequence until the curvature and the flow rate reach to the inlet condition at the top of the evaporator. In the present study, curvature radius and bulk flow rate are set as $R(0) = 4\times10^{-8}$ (m) and $\dot{G}(0) = 0$ (kg/m^{2}s) at the origin x=0.

PREDICTION OF FALLING FILM EVAPORATOR

First, the gravitational effect is investigated by inclining the evaporator wall. Again R123 is adopted with T_w=303.15K and T_{sat}=298.15K. Figure 9 shows the liquid length l inside the groove plotted against groove width w. Liquid length l is defined as the length between the inlet where the groove is filled with inscribed meniscus and the point where the liquid dries out (see Fig. 10). When the surface is placed horizontally (φ=0deg), the grooves easily dry out. Surface tension pulls the liquid along the groove to some extent, but it is unsatisfactory for supplying enough liquid to wide area of heat transfer surface. This means that it is necessary to introduce a mechanism other than surface

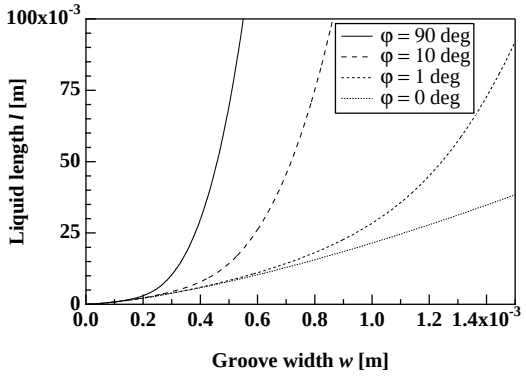

Fig. 9 Liquid length inside the groove

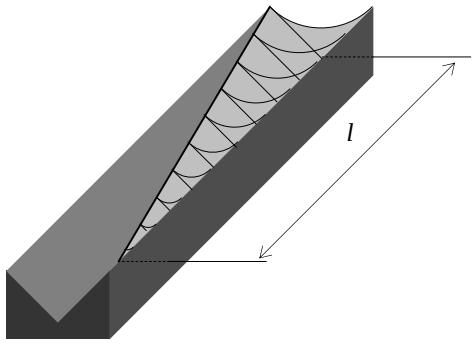

Fig. 10 Schematic view of liquid length l

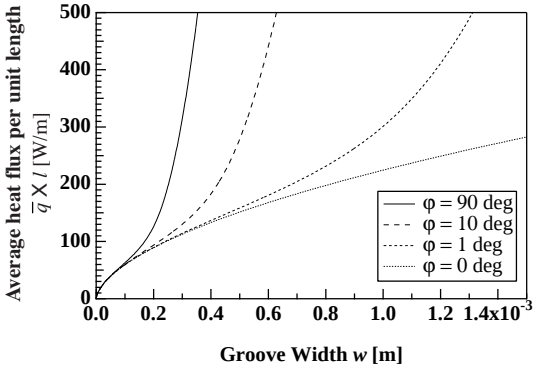

Fig. 11 Total heat evaporated from unit width

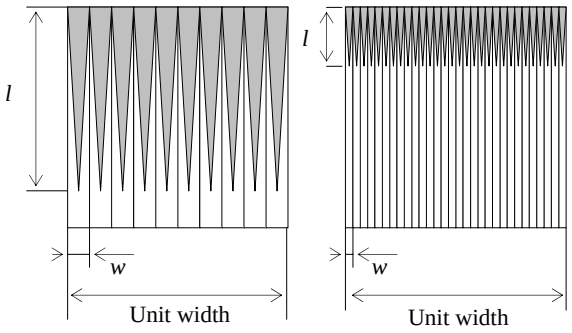

Fig. 12 Evaporator surface with large grooves and small grooves

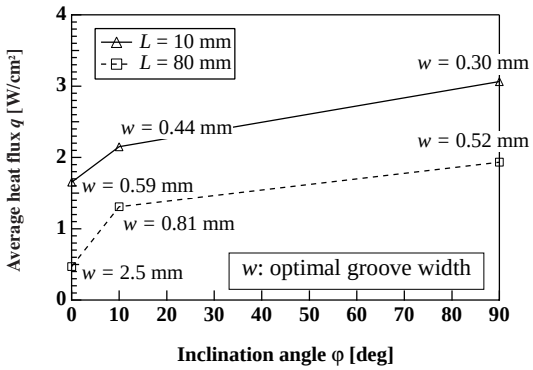

Fig. 13 Average heat flux for different evaporator length L

tension to pull the liquid sufficiently into the micro groove. As the heat transfer surface is further inclined and the groove gets upright, gravity effectively pulls down the flow and the liquid length is increased. Thus, it is confirmed that the gravitational force is essential for providing the liquid to large heat transfer area. As the groove width gets smaller (w<200μm), surface tension effect becomes dominant again and the liquid is consumed by strong evaporation. This large consumption of the liquid makes the liquid length very short even for large inclination angle cases.

Figure 11 shows the total heat evaporated from unit width of the falling film evaporator (=averaged heat flux $\overline{q}$ $\times$ liquid length l, W/m) plotted against groove width. The curves show monotone increase against groove width, which indicates that large grooves that can supply liquid longer is better than small grooves that easily dry out. Figure 12 is a sketch of the heat transfer surface with large grooves and small grooves. Since smaller grooves have many interline regions per area, they can produce higher local heat flux than larger grooves at wetted area. However, the present result reveals that it is better to supply liquid to wider area by large grooves to eliminate the dry out area, even though the local heat flux is deteriorated at the wetted area.

Figures 11 and 12 imply that maximum heat exchange can be achieved when the liquid just dries out at the bottom of the falling film evaporator. Figure 13 shows the averaged heat flux of the whole evaporator surface of length L. Groove width is optimized for each case so that the evaporator surface becomes all wet and the liquid just dries out at the bottom. The values of optimal groove width are also plotted in the figure. Optimal width gets smaller as the surface is inclined. Smaller length L and larger inclination angle φ give larger heat flux. Furthermore, average heat flux becomes more insensitive to the inclination angle as length L gets smaller.

DIVERGING BRANCH EVAPORATOR

Previous results come up with the idea that two important functions, i.e. liquid supply by gravity and the liquid consumption by strong evaporation, should be individually realized in the micro groove falling film evaporator design. In relatively large grooves, gravitational force can effectively flush large amount of liquid, while surface tension force can strongly pull the liquid into the narrow grooves to the strong evaporating region. Thus, diverging branch evaporator is investigated. Bifurcated branching is adopted for simplicity in the present study. The liquid is first supplied into the wide primary groove in the gravitational direction, and then the fluid is pulled horizontally into the small second grooves and consumed by effective evaporation. The schematic of diverging branch system is shown in Fig. 14. At the connection point of the branches, same curvature radius was simply adopted in the calculation.

The groove width and length of the horizontal branch are fixed as w_2=50μm and L_2=314.8μm, respectively. The primary groove width w_1 is optimized so that the whole evaporator surface of length L_1 gets wet. Figure 15 shows the averaged heat flux for diverging branch heat exchanger. It can be seen that diverging branch evaporator shows nearly twice as large heat flux than the standard groove evaporator of same length (see Fig. 13).

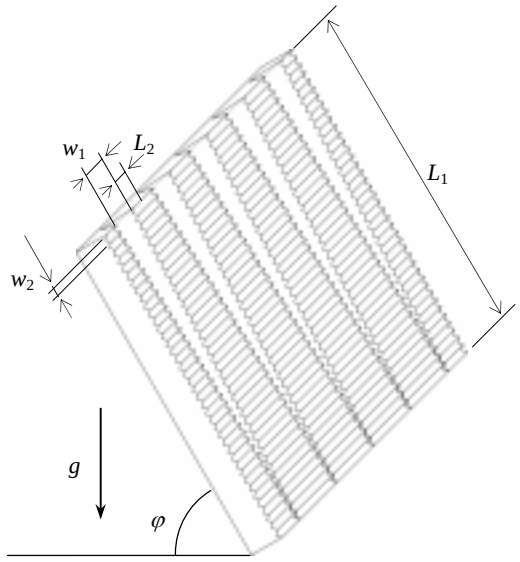

Fig. 14 Schematic view of the diverging branch evaporator

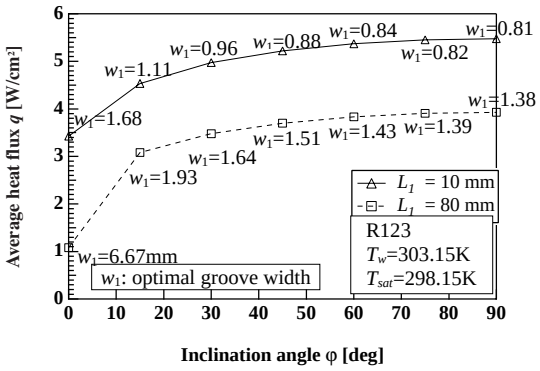

Fig. 15 Average heat flux of diverging branch evaporator

It must be noted that this result was obtained without any optimization for the small horizontal branch width w_2. Moreover, it is known that trapezoidal grooves will give better performance than triangular grooves. Different refrigerant with larger thermal conductivity will also drastically increase the heat flux. Thus there is certainly room for further improvement. It can be said that diverging branch evaporator has large potentiality for improving micro groove falling film evaporator performance.

CONCLUSIONS

1. Heat transfer in a falling film micro groove evaporator is simulated by an analytical model. The model described by Stephan and Busse (1992) is employed for the micro region, and it is combined with the macro region model that takes into account the gravitational, surface tension and viscous forces.
2. Gravity can effectively pull down the fluid inside the groove, and can drastically enhance the wetting of the surface. As the groove width gets smaller, surface tension gets dominant, and effective evaporation can be achieved.
3. Maximum heat exchange can be obtained when the liquid just dries out at the bottom of the falling film evaporator.
4. Diverging branch evaporator showed nearly twice as large heat flux than the standard groove evaporator of same length. It is concluded that diverging branch evaporator has large potentiality for improving the performance of the micro groove falling film evaporator.

NOMENCLATURE

A	dispersion constant, J, or area, m^2
D	hydraulic diameter, m
f	evaporation coefficient, dimensionless, or friction factor, dimensionless
$\dot{G}$	macro region mass flow rate, kg/m^2s
$\dot{g}$	macro region evaporation rate, kg/m^2s
h_{fg}	specific heat of evaporation, J/kg
K	curvature of the meniscus, 1/m
L	evaporator length, m
l	liquid length inside the groove, m
$\dot{M}$	micro region mass flow rate, kg/m^2s
$\dot{m}$	micro region evaporation rate, kg/m^2s
p	pressure, Pa
q	heat flux, W/m^2
R	curvature radius, m
R_g	gas constant J/kgK
S	perimeter, m
T	temperature, K
w	groove width, m
x	direction of the groove, m
δ	film thickness, m
η	viscosity, Pa s,
φ	inclination angle, rad
λ	thermal conductivity, W/mK
ν	kinematic viscosity, m^2/s
θ	film thickness gradient at macro-micro boundary, rad
ρ	density, kg/m^3
σ	surface tension, N/m
ξ	flow direction in the micro region, m
ζ	distance from the wall, m

Subscript

c	capillary
iv	vapor side of the liquid-vapor interface
l	liquid
m	mean
s	solid
sat	saturation
v	vapor
1	primary branch
2	horizontal branch

REFERENCES

Kamotani, Y., 1978, Evaporator film coefficients of grooved heat pipes, *Proc. 3rd Int. Heat Pipe Conf.*, Palo Alto.

Spedding, P. L. and Hand, N. P., 1997, Prediction in stratified gas-liquid co-current flow in horizontal pipelines, *Int. J. Heat Mass Transfer*, Vol. 40, pp.1923-1935.

Stephan, P. and Busse, C. A., 1992, Analysis of the heat transfer coefficient of grooved heat pipe evaporator walls, *Int. J. Heat Mass Transfer*, Vol. 35, pp.383-391.

Taitel, Y. and Duckler, A. E., 1976, A theoretical approach to the Lockhart-Martinelli correlation for stratified flow, *Int. J. Multiphase Flow*, Vol. 2, pp.591-595.

Wayner, P. C., Jr., Kao, Y. K. and LaCroix, L. V., 1976, The interline heat-transfer coefficient of an evaporating

wetting film, *Int. J. Heat Mass Transfer*, Vol. 19, pp. 487-492.

Wayner, P. C., Jr., 1982, Adsorption and capillary condensation at the contact line in change of phase heat transfer, *Int. J. Heat Mass Transfer*, Vol. 25, pp. 707-713.

Wayner, P. C., Jr., 1997, Interfacial Forces and Phase Change in Thin Liquid Films, in *Microscale Heat Transfer*, Edited by C.L. Tien, F.W. Gerner, and A. Majumdar, Taylor & Francis, New York, Chapter 6, pp. 187-226.

Wayner, P. C., Jr., 1999, Intermolecular forces in phase-change heat transfer: 1998 Kern Award Review, *AIChE J.*, Vol. 45, pp. 2055-2068.